On the Observed Relationships between Variability in Kuroshio-Oyashio Sea Surface Temperatures and the Atmospheric Circulation over the North Pacific

Samantha M. Wills* and David W. J. Thompson

Department of Atmospheric Science, Colorado State University, Fort Collins, CO 80521

Submitted to J. Climate, May 2017

Revised manuscript submitted to J. Climate, June 2017

*Corresponding author address: Samantha M. Wills, Department of Atmospheric Science, Colorado State University, Fort Collins, CO 80521

E-mail: smwills@atmos.colostate.edu

10 **ABSTRACT**

11 Observational analyses reveal that variations in sea surface temperatures (SST) in the
12 Kuroshio-Oyashio extension (KOE) region of the North Pacific are associated with two dis-
13 tinct and robust patterns of atmospheric variability: 1) a pattern that peaks in amplitude
14 approximately 2 - 3 weeks prior to large KOE SST anomalies, and is consistent with atmo-
15 spheric forcing of the SST field and 2) a very different pattern that lags SST anomalies in
16 the KOE region by approximately a month. The latter pattern is dominated by low sea level
17 pressure anomalies located over warm SST anomalies, and is interpreted as the transient
18 atmospheric response to SST anomalies over the KOE region. The results contribute to a
19 growing body of evidence that suggests variations in SSTs in the midlatitude oceans are
20 capable of significantly influencing the large-scale atmospheric circulation, especially near
21 western boundary currents.

I. Introduction

The Earth's climate is characterized by coupled atmosphere, ocean, land surface, and sea ice systems, and the internal interactions between these systems are key to understanding climate variability. The two-way interactions between the ocean and the atmosphere are of particular interest, as the ability to predict changes to the atmospheric circulation based on changes in sea surface temperature (SST) can significantly improve forecasting skill. While the atmospheric response to SST anomalies is well understood in certain regions of the globe [i.e., the Tropics], the extent to which the atmosphere responds to variations in midlatitude SSTs remains an ongoing topic of research. In the midlatitudes, air-sea interaction is typically dominated by atmosphere-to-ocean forcing [e.g., Davis 1976, 1978; Deser and Timlin 1997; Ciasto and Thompson 2004], and the influence of the ocean on the atmosphere has (previously) been thought to be small in comparison to internal atmospheric variability [e.g., Palmer and Sun 1985; Barsugli and Battisti 1998; Kushnir et al. 2002]. From a thermodynamic perspective, the heat fluxes associated with midlatitude SST anomalies are readily balanced by modest changes in the low-level meridional wind since the north-south gradients in temperature are relatively large [e.g., Hoskins and Karoly 1981]. As such, we would expect the atmospheric response to anomalous surface heating to be confined to the lowermost troposphere and have little impact on the large-scale atmospheric circulation.

Recent advancements in the resolution of satellite observations and numerical models over the past decade have provided new evidence that suggests the midlatitude ocean has a potentially important impact on the atmospheric circulation in regions of large horizontal SST gradients. Observations of wind stress curl and divergence from the QuikSCAT satellite radar scatterometer [e.g., Chelton et al. 2001] indicated that surface air blowing across an ocean front (or a region of large horizontal SST gradients) tended to accelerate the wind, leading to patterns of convergence and divergence at the surface [e.g., O'Neill et al. 2003; Nonaka and Xie 2003; Chelton et al. 2004; Chelton and Xie 2010]. Observational and numerical studies have shown that the *climatological-mean* SST gradients associated with

the major western boundary currents are capable of forcing vertical motion (i.e., through changes in the near-surface wind field) well into the free troposphere [e.g., Minobe et al. 2008, 2010] and influencing the strength and position of the extratropical storm tracks [e.g., Nakamura et al. 2008; Sampe et al. 2010; Small et al. 2014; Piazza et al. 2016].

A growing body of work suggests that *variations* in midlatitude SSTs can also have a significant impact on the atmospheric circulation. For example, observational studies have found that significant patterns of SST anomalies precede changes in the North Atlantic Oscillation on timescales of months [e.g., Czaja and Frankignoul 2002] to weeks [e.g., Ciasto and Thompson 2004]. Other observational studies have shown that meridional shifts in the locations of the Kuroshio-Oyashio and Gulf Stream extension fronts are significantly linked to variations in the large-scale atmospheric circulation on both interannual and intraseasonal timescales [e.g., Frankignoul et al. 2011; Kwon and Joyce 2013]. Both numerical [e.g., Brayshaw et al. 2008; Hand et al. 2014; Michel and Rivieré 2014] and observational [e.g., Nakamura and Yamane 2009; O'Reilly and Czaja 2015] studies have indicated that variations in midlatitude SST gradients are capable of influencing the amplitudes and locations of the storms tracks. A numerical experiment run with a high-resolution atmospheric general circulation model suggested that positive SST anomalies over the Kuroshio-Oyashio extension lead changes in vertical motion by several weeks [e.g., Smirnov et al. 2015], consistent with studies that have linked anomalously warm SSTs in the Gulf Stream region to vertical motion in the warm sector of extratropical storms [e.g., Czaja and Blunt 2011; Sheldon and Czaja 2013].

In a recent paper [Wills et al. 2016], we examined the observational evidence for midlatitude air-sea interaction over the Gulf Stream region using lead/lag regressions based on daily-mean data. The analyses revealed that atmosphere-ocean interaction over the Gulf Stream region is associated with two statistically significant and distinct patterns of atmospheric circulation anomalies: one that leads variations in Gulf Stream SSTs by several weeks, and one that lags Gulf Stream SSTs. The latter pattern suggests that warm SST

anomalies in the Gulf Stream extension lead to anomalously low pressure directly over the SST anomalies and high pressure to the northeast.

Here we examine the evidence for analogous interactions over the Kuroshio-Oyashio extension (KOE). A key result is that - as is the case with SST anomalies in the North Atlantic - SST anomalies in the KOE are associated with two distinct and seemingly independent patterns of atmospheric variability: 1) a pattern that leads the SST field and is consistent with atmospheric forcing of the ocean and 2) a pattern that lags the SST field and may be interpreted as the atmospheric response to midlatitude ocean forcing. The most robust component of the lagged response over both ocean basins is anomalous low surface pressure centered over the warm SST anomalies. Section 2 provides a description of the data. Section 3 explores the observed lead-lag relationships between the atmospheric circulation and SSTs in the KOE. Section 4 compares the KOE results with results based on SST anomalies in the Gulf Stream extension from the companion paper [Wills et al. 2016], and conclusions are provided in section 5.

II. Data

The observational analyses are based on daily-mean output from the ERA-Interim Reanalyses examined here on a 1.5°-resolution grid over the 35-yr period 1979 - 2013 [e.g., Dee et al. 2011; https://apps.ecmwf.int/datasets/data/interim-full-daily]. The data are detrended to remove the influence of trends on the results, and anomalies in SST, potential temperature (θ), wind (v), and geopotential height (Z) were formed by removing the long-term mean seasonal cycle from the data at all grid points. Note that, throughout this study, sea level pressure (SLP) is expressed as geopotential height at 1000 hPa (Z_{1000}). Apart from the removal of the seasonal cycle and the detrending, the data are not filtered in any way in the analyses. The statistical significance of key results is shown in Figure 3, and details of the significance test are provided in the caption.

III. Observed lead/lag relationships

a. Results based on a SST index

To provide context for the analyses, we show in Figure 1 a brief synopsis of the NH wintertime-mean (Dec - Feb) circulation and SST field over the North Pacific. Figure 1a shows the climatological-mean DJF SST and 850 hPa horizontal wind fields; Fig. 1b shows the associated climatological standard deviation of the daily-mean SST field. Based on the standard deviation in the SST field, it is evident that there are two primary regions of enhanced SST variability in the North Pacific: one to the east of Japan and one in the southeastern North Pacific. Our primary focus is on the region to the east of Japan (indicated by the box in Fig. 1b), which is associated with variability in the KOE [e.g., Nonaka and Xie 2003; Frankignoul et al. 2011; Smirnov et al. 2015], and is where approximately 40% - 60% of SST variability is intrinsic to the ocean [e.g., Smirnov et al. 2014]. The second region of large SST variance (centered near 160°W) is linked to the extratropical atmospheric response to ENSO [e.g., Alexander 1992; Cayan 1992; Diaz et al. 2001] and is not the focus of the current study. The potential contamination of our results by ENSO variability is discussed later in this section.

We investigate the two-way interactions between variations in KOE SSTs and the atmospheric circulation using lead/lag analysis, similar to the technique used in [Wills et al. 2016]. To capture the SST variability associated with the KOE (i.e., the variance maximum to the east of Japan in Fig. 1b), we create a time series of daily-mean SST anomalies averaged over the region 36°N - 42°N, 140°E - 171°E (indicated by the box in Fig. 1b). The index (hereafter $\mathsf{K}_{\mathsf{SST}}$) is standardized so that it has a mean of zero and standard deviation of one, where positive values of the index correspond to positive SST anomalies in the KOE region, and vice versa. Note that - like the definition of the Gulf Stream region in [Wills et al. 2016] - the results are not sensitive to the specific domain used to define the KOE region.

To analyze the relationships between KOE SST anomalies and the anomalous atmospheric circulation, we regressed various atmospheric fields against the $\mathsf{K}_{\mathsf{SST}}$ index on

daily-mean timescales at lags spanning -30 to +30 days. By construction, the $\mathsf{K}_{\mathsf{SST}}$ index is always centered on the 90-day period from 1 December - 28 February, and negative (positive) lags indicate results where the fields being regressed precede (follow) the largest KOE SST anomalies. Hence, at a lag of -30 days (+30 days), the fields being regressed are centered on the 90-day period from 1 November - 29 January (31 December - 30 March). The statistical significance of the SLP anomalies at lags of -30 and +30 days is also calculated to assess the robustness of the SLP regression patterns at negative and positive lag (Fig. 3).

The lag regressions in the left column of Fig. 2 highlight the evolution of the anomalous surface atmospheric circulation associated with SST anomalies in the KOE region on daily-mean timescales. Regression coefficients of SST (shading) and SLP (contours) are shown every 15 days between lags of -30 and +30 days. As per the definition of the $\mathsf{K}_{\mathsf{SST}}$ index, anomalously warm SSTs peak in amplitude over the KOE region at a lag of zero days, and the results show strong persistence in the anomalous SST field through all lags (consistent with the large heat capacity of the ocean). Based on the regressions at negative lag (i.e., when the fields *precede* the largest KOE SST anomalies), it is evident that the warmest SST anomalies are formed by positive SLP anomalies that span much of the North Pacific basin. Specifically, the anomalous surface atmospheric circulation in the top left panel of Fig. 2 acts on the climatological-mean SST gradient in Fig. 1a to advect anomalously warm air from the east/southeast over the KOE region. As observed for the Gulf Stream in [Wills et al. 2016] and documented in previous literature [e.g., Deser and Timlin 1997; Kushnir et al. 2002; Ciasto and Thompson 2004], this result is consistent with atmospheric forcing of the SST field. The results at positive lag (i.e., when the fields *follow* the largest KOE SST anomalies) indicate that anomalously warm SSTs are followed by a very different pattern of atmospheric circulation anomalies. At positive lag, the circulation anomalies are dominated by low SLP anomalies that overlie and extend downstream of the KOE region. The anomalies also include anomalously high SLP centered (approximately) between Alaska and Kamchatka, but as noted below, the high pressure feature is not significant.

The associated structures in the 200 hPa geopotential height and $Z_{200} - Z_{1000}$ fields (right column) reveal that: 1) the circulation anomalies at negative lag amplify with height and are associated with positive thickness anomalies that extend through the depth of the troposphere and 2) the circulation anomalies at positive lag are associated with much weaker thickness anomalies and are thus relatively confined to lower levels.

The significance of the anomalous circulation patterns at negative and positive lags is shown in Fig. 3. As expected from previous analyses based on pentad and weekly-mean SST data [e.g., Deser and Timlin 1997; Ciasto and Thompson 2004], the most significant SLP and Z_{200} anomalies are found at negative lags (top panels in Fig. 3), when - as discussed above - the atmospheric circulation anomalies are consistent with forcing of the SST field. At positive lag, the low pressure center of action is most significant at the surface. The weak center of high pressure to the north of the KOE region is not significant at any level.

As noted earlier, ENSO has a marked influence on the North Pacific SST field [e.g., Alexander 1992]. However, and importantly, it does not contribute to the results shown here. The influence of ENSO was tested as follows: 1) we defined ENSO as the standardized time series of daily-mean SST anomalies averaged over the region 6°S - 6°N, 171°W - 120°W (i.e., Nino 3.4). 2) We linearly regressed the ENSO index from the SLP time series at each grid point to form the ENSO-residual SLP data. The fits were done for the SLP field lagging the ENSO index by 40 days. And 3) we repeated the analyses in Fig. 2 using the ENSO-residual SLP data. Removing ENSO from the SLP data did not change the overall patterns or significance of the results. This is expected since ENSO is unlikely to contribute to the day-to-day evolution of the North Pacific SLP field, and thus is unlikely to influence the evolution of the SLP anomalies shown in Fig. 2.

b. Results based on an atmospheric index

Analyses based on the K_{SST} index indicate a significant and distinct pattern of atmospheric circulation anomalies at positive lag, but it is unclear if this pattern is dependent

on SST anomalies within the KOE region. While the SLP pattern at positive lag may arise due to the presence of persisting SST anomalies, it may also arise from the independent evolution of the anomalous atmospheric circulation observed at negative lag. As done in the companion paper [Wills et al. 2016], we tested against the latter possibility by repeating the analyses in Fig. 2, but for regressions based on the expansion coefficient time series of the "atmospheric forcing" pattern (that is: the pattern of circulation anomalies at negative lags). The "atmospheric forcing" time series (hereafter $\mathsf{K}_{\mathsf{ATMO}}$) was created by calculating the cosine-weighted average of daily-mean SLP anomalies over the region 150°E - 171°W, 39°N - 54°N (i.e., near the center of action of the SLP anomalies) for all days 1979 - 2013 and then standardizing the resulting index. By construction, the $\mathsf{K}_{\mathsf{ATMO}}$ index indicates the temporal evolution of the anomalous atmospheric circulation observed at negative lags (top-left panels of Fig. 2) that does not depend on (direct) information from the SST field. To compare against the results based on the $\mathsf{K}_{\mathsf{SST}}$ index, we regressed SST and SLP onto $\mathsf{K}_{\mathsf{ATMO}}$ at 15-day intervals for lags spanning 0 to +60 days. Hence, lags of 0, +15, +30, +45, and +60 days from the $\mathsf{K}_{\mathsf{ATMO}}$ regressions directly correspond to lags of -30, -15, 0, +15, and +30 days from the $\mathsf{K}_{\mathsf{SST}}$ regressions, respectively.

The lag regressions of SST and SLP onto $\mathsf{K}_{\mathsf{ATMO}}$ are shown in Fig. 4. The results indicate that the $\mathsf{K}_{\mathsf{ATMO}}$ index projects onto SST anomalies over the KOE region, as expected from results based on the $\mathsf{K}_{\mathsf{SST}}$ index (Fig. 2). The results also indicate that the SLP anomalies associated with the atmospheric index decay quickly over a time period of a few weeks and (most importantly) do *not* evolve into the pattern of SLP anomalies that lag the $\mathsf{K}_{\mathsf{SST}}$ index. Thus, the evolution of the "atmospheric forcing" pattern appears to be independent of the anomalous atmospheric circulation that forms approximately a month after peak KOE SST anomalies. Furthermore, the results suggest that the unique pattern of circulation anomalies found at positive lags in Fig. 2 derives from information unique to the SST field, as also observed in similar results for the Gulf Stream in [Wills et al. 2016].

IV. Comparison with results based on SST anomalies in the Gulf Stream extension

The observational results presented in this study have indicated that there are two very different and independent patterns of atmospheric circulation anomalies that lead and lag variations in KOE SSTs in the North Pacific on daily-mean timescales. The first pattern, which leads the largest KOE SST anomalies by several weeks, is characterized by statistically significant high pressure anomalies that span much of the North Pacific basin, and is consistent with atmospheric forcing of the ocean. The second pattern, which lags the largest KOE SST anomalies by approximately a month, is characterized by statistically significant low pressure anomalies that are coincident with positive SST anomalies in the KOE region, and are most significant and robust at the surface. The observational results presented here are broadly similar to those found for SST anomalies in the Gulf Stream extension region in the companion paper [Wills et al. 2016], as discussed in more detail below.

In the companion paper [Wills et al. 2016], the same observational analyses were performed but for an index of North Atlantic SSTs averaged over the Gulf Stream extension. Figure 5 compares the SST and SLP fields regressed onto the $\mathsf{K}_{\mathsf{SST}}$ index used here (left) and the Gulf Stream extension index ($\mathsf{G}_{\mathsf{SST}}$; right) (see [Wills et al. 2016] for details of the analyses). As in Fig. 2, lags span from -30 to +30 days, with negative lags indicating results where the SLP and SST fields precede peak amplitude in the SST index, and vice versa. In both the North Pacific and North Atlantic, positive SST anomalies in the western boundary current regions are preceded by circulation anomalies that are consistent with anomalous warm air advection over the western boundary current regions. The largest SST anomalies in each basin are of comparable amplitude and decay slowly over time. The circulation anomalies at negative lags are of similar magnitude and size and peak approximately 15 - 20 days prior to the strongest SST anomalies in both basins.

Importantly, the circulation anomalies at positive lag are also very similar over both ocean basins (bottom panels of Fig. 5). In particular, both basins exhibit anomalously low

SLP centered approximately over the SST anomalies. The high pressure anomalies found at positive lag over the North Atlantic sector are not significant in results for the North Pacific sector. *Hence, we view the anomalous low pressure pattern that develops over the SST anomalies to be the most robust common aspect of the atmospheric "response" over both ocean basins.*

V. Conclusions

In the current study and the companion paper [Wills et al. 2016], we investigated the observed daily-mean relationships between the atmospheric circulation and SST anomalies in the vicinity of the major Northern Hemisphere western boundary currents. Together, the two studies suggest that SST anomalies in the Gulf Stream and Kuroshio-Oyashio extensions are both associated with distinct patterns of atmospheric variability that precede and follow peak amplitude in the SST field. Prior to the onset of peak SST anomalies, both basins exhibit similar "atmospheric forcing" patterns that are consistent with anomalous temperature advection due to the anomalous flow acting on the climatological-mean SST gradient. Following peak amplitude in the SST anomalies, both basins exhibit a distinct pattern of pressure anomalies centered over and to the east of the western boundary currents: warm SST anomalies are associated with low SLP anomalies that do not notably amplify with height. The most notable difference in the lagged patterns between the ocean basins is the absence of significant out of phase pressure anomalies to the north of the SST anomalies over the Pacific sector.

We argue that the pattern of low pressure anomalies at positive lag potentially reflects the "atmospheric response" to midlatitude SST anomalies based on the following evidence:

1. Results based on analyses over both the Kuroshio-Oyashio and Gulf Stream extensions in the North Pacific and North Atlantic both yield very similar "response" patterns (Fig. 5).

2. Over both basins, the pattern of circulation anomalies at positive lag (the "response")

has a very different spatial structure than the pattern at negative lag (the "forcing") (Fig. 2 here and Fig. 2 from [Wills et al. 2016]).

3. The pattern is statistically significant over both ocean basins (Fig. 3 here and Fig. 3 from [Wills et al. 2016]).

4. The pattern does not emerge from analyses based on the evolution of the atmospheric circulation in the absence of (direct) information from the SST field (Fig. 4 here and Fig. 5 from [Wills et al. 2016]).

The formation of low sea level pressure anomalies at positive lag over and slightly east of warm SST anomalies is broadly consistent with the theoretical linear response to midlatitude SST anomalies [e.g., Hoskins and Karoly 1981]. We are currently designing numerical experiments that will explore the physical mechanisms of the responses indicated here in greater detail. The results of those experiments will be explored in a future paper.

Acknowledgments. S.M.W. is funded by the NASA Physical Oceanography program under Grant NNX13AQ04G. D.W.J.T. is funded by the NASA Physical Oceanography program and the NSF Climate Dynamics program under Grant AGS-1343080.

REFERENCES

Alexander, M.A., 1992: Midlatitude Atmosphere-Ocean Interaction during El Niño. Part I: The North Pacific Ocean. *J. Climate*, **5**, 944 - 958.

Barsugli, J.J., and D.S. Battisti, 1998: The Basic Effects of Atmosphere-Ocean Thermal Coupling on Midlatitude Variability. *J. Atmos. Sci.*, **55**, 477 - 493.

Brayshaw, D.J., B. Hoskins, and M. Blackburn, 2008: The Storm-Track Response to Idealized SST Perturbations in an Aquaplanet GCM. *J. Atmos. Sci.*, **65**, 2842 - 2860.

Cayan, D.R., 1992: Latent and Sensible Heat Flux Anomalies over the Northern Oceans: Driving the Sea Surface Temperature. *J. Phys. Oceanogr.*, **22**, 859 - 881.

Chelton, D.B., S.K. Esbensen, M.G. Schlax, N. Thum, M.H. Freilich, F.J. Wentz, C.L. Gentemann, M.J. McPhaden, and P.S. Schopf, 2001: Observations of Coupling between Surface Wind Stress and Sea Surface Temperature in the Eastern Tropical Pacific. *J. Climate*, **14**, 1479 - 1498.

Chelton, D.B., M.G. Schlax, M.H. Freilich, and R.F. Milliff, 2004: Satellite Measurements Reveal Persistent Small-Scale Features in Ocean Winds. *Science*, **303**, 978 - 983.

Chelton, D.B., and S.-P. Xie, 2010: Coupled ocean-atmosphere interaction at oceanic mesoscales. *Oceanography*, **23**, 52 - 69.

Ciasto, L.M., and D.W.J. Thompson, 2004: North Atlantic Atmosphere-Ocean Interaction on Intraseasonal Time Scales. *J. Climate*, **17**, 1617 - 1621.

Czaja, A., and C. Frankignoul, 2002: Observed Impact of Atlantic SST Anomalies on the North Atlantic Oscillation. *J. Climate*, **15**, 606 - 623.

Czaja, A., and N. Blunt, 2011: A new mechanism for ocean-atmosphere coupling in midlatitudes. *Q. J. R. Meteorol. Soc.*, **137**, 1095 - 1101.

Davis, R.E., 1976: Predictability of Sea Surface Temperature and Sea Level Pressure Anomalies over the North Pacific Ocean. *J. Phys. Oceanogr.*, **6**, 249 - 266.

Davis, R.E., 1978: Predictability of Sea Level Pressure Anomalies Over the North Pacific Ocean. *J. Phys. Oceanogr.*, **8**, 233 - 246.

Dee, D.P., S.M. Uppala, A.J. Simmons, P. Berrisford, P. Poli, S. Kobayashi, U. Andrae, M.A. Balmaseda, G. Balsamo, P. Bauer, P. Bechtold, A.C.M. Beljaars, L. van de Berg, J. Bidlot, N. Bormann, C. Delsol, R. Dragani, M. Fuentes, A.J. Geer, L. Haimberger, S.B. Healy, H. Hersbach, E.V. Holm, L. Isaksen, P. Kallberg, M. Kohler, M. Matricardi, A.P. McNally, B.M. Monge-Sanz, J.-J. Morcrette, B.-K. Park, C. Peubey, P. de Rosnay, C. Tavolato, J.-N. Thepaut, and F. Vitart, 2011: The ERA-Interim reanalysis: configuration and performance of the data assimilation system. *Q. J. R. Meteorol. Soc.*, **137**, 553 - 597.

Deser, C., and M.S. Timlin, 1997: Atmosphere-Ocean Interaction on Weekly Timescales in the North Atlantic and Pacific. *J. Climate*, **10**, 393 - 408.

Diaz, H.F., M.P. Hoerling, and J.K. Eischeid, 2001: ENSO Variability, Teleconnections and Climate Change. *Int. J. Climatol.*, **21**, 1845 - 1862.

Frankignoul, C., N. Sennechael, Y-O. Kwon, and M.A. Alexander, 2011: Influence of the Meridional Shifts of the Kuroshio and the Oyashio Extensions on the Atmospheric Circulation. *J. Climate*, **24**, 762 - 777.

Hand, R., N. Keenlyside, N.-E. Omrani, M. Latif, 2014: Simulated response to inter-annual SST variations in the Gulf Stream region. *Clim. Dyn.*, **42**, 715 - 731.

Hoskins, B.J., and D.J. Karoly, 1981: The Steady Linear Response of a Spherical Atmosphere to Thermal and Orographic Forcing. *J. Atmos. Sci.*, **38**, 1179 - 1196.

Kushnir, Y., W.A. Robinson, I. Blade, N.M.J. Hall, S. Peng, and R. Sutton, 2002: Atmospheric GCM Response to Extratropical SST anomalies: Synthesis and Evaluation. *J. Climate*, **15**, 2233 - 2256.

Kwon, Y.-O., and T. M. Joyce, 2013: Northern Hemsiphere Winter Atmospheric Transient Eddy Heat Fluxes and the Gulf Stream and Kuroshio-Oyashio Extension Variability. *J. Climate*, **26**, 9839 - 9859.

Michel, C. and G. Rivieré, 2014: Sensitivity of the Position and Variability of the Eddy-Driven Jet to Different SST Profiles in an Aquaplanet General Circulation Model. *J. Atmos. Sci.*, **71**, 349 - 371.

Minobe, S., A. Kuwano-Yoshida, N. Komori, S-P. Xie, and R.J. Small, 2008: Influence of the Gulf Stream on the troposphere. *Nature*, **452**, 206 - 210.

Minobe, S., M. Miyashita, A. Kuwano-Yoshida, H. Tokinaga, and S-P. Xie, 2010: Atmospheric Response to the Gulf Stream: Seasonal Variations. *J. Climate*, **23**, 3699 - 3719.

Nakamura, H., T. Sampe, A. Goto, W. Ohfuchi, and S-P. Xie, 2008: On the importance of midlatitude oceanic frontal zones for the mean state and dominant variability in the tropospheric circulation. *Geophys. Res. Lett.*, **35**, L15709, doi:10.1029/2008GL034010.

Nakamura, M., and S. Yamane, 2009: Dominant Anomaly Patterns in the Near-Surface Baroclinicity and Accompanying Anomalies in the Atmosphere and Oceans. Part I: North Atlantic Basin. *J. Climate*, **22**, 880 - 904.

Nonaka, M., and S-P. Xie, 2003: Covariations of Sea Surface Temperature and Wind over the Kuroshio and Its Extension: Evidence for Ocean-to-Atmosphere Feedback, *J. Climate*, **16**, 1404 - 1413.

O'Neill, L.W., D.B. Chelton, and S.K. Esbensen, 2003: Observations of SST-Induced Perturbations of the Wind Stress Field over the Southern Ocean on Seasonal Timescales. *J. Climate*, **16**, 2340 - 2354.

O'Reilly, C.H., and A. Czaja, 2015: The response of the Pacific storm track and atmospheric circulation to Kuroshio Extension variability. *Q. J. R. Meteorol. Soc.*, **141**, 52 - 66.

Palmer, T.N., and Z. Sun, 1985: A modelling and observational study of the relationship between sea surface temperature in the north-west Atlantic and the atmospheric general circulation. *Q. J. R. Meteorol. Soc.*, **111**, 947 - 975.

Piazza, M., L. Terray, J. Boé, E. Maisonnave, E. Sanchez-Gomez, 2015: Influence of small-scale North Atlantic sea surface temperature patterns on the marine boundary layer and free troposphere: a study using the atmospheric ARPEGE model. *Clim. Dyn.*, DOI 10.1007/s00382-015-2669-z.

Sampe, T., H. Nakamura, A. Goto, and W. Ohfuchi, 2010: Significance of a Midlatitude SST Frontal Zone in the Formation of a Storm Track and an Eddy-Driven Westerly Jet. *J. Climate*, **23**, 1793 - 1814.

Sheldon, L., and A. Czaja, 2013: Seasonal and interannual variability of an index of deep atmospheric convection over western boundary currents. *Q. J. R. Meteorol. Soc.* DOI:10.1002/qj.2103.

Small, R.J., R.A. Tomas, F.O. Bryan, 2014: Storm track response to ocean fronts in a global high-resolution climate model. *Clim. Dyn.*, DOI 10.1007/s00382-013-1980-9.

Smirnov, D., M. Newman, and M.A. Alexander, 2014: Investigating the Role of Ocean-Atmosphere Coupling in the North Pacific Ocean. *J. Climate*, **27**, 592 - 606.

Smirnov, D., M. Newman, M.A. Alexander, Y-O. Kwon, and C. Frankignoul, 2015: In-

vestigating the Local Atmospheric Response to a Realistic Shift in the Oyashio Sea Surface Temperature Front. *J. Climate*, **28**, 1126 - 1147.

Wills, S.W., D.W.J. Thompson, L.M. Ciasto, 2016: On the Observed Relationships between Variability in Gulf Stream Sea Surface Temperatures and the Atmospheric Circulation over the North Atlantic. *J. Climate*, **29**, 3719 - 3730.

Figure Captions

Figure 1: Climatological values of North Pacific wintertime (DJF) a) SST (contours) and $\vec{\mathsf{u}}_{850}$ (vectors) and b) standard deviation of SST (σ_{SST}). The boxed region spans $36°\mathsf{N} - 42°\mathsf{N}, 140°\mathsf{E} - 171\mathsf{E}°$ and indicates the region used to calculate the $\mathsf{K}_{\mathsf{SST}}$ index. Units for SST and σ_{SST} are in Kelvin. Units for $\vec{\mathsf{u}}$ are in m/s.

Figure 2: Wintertime lag regressions of (left column) Z_{1000} and SST and (right column) Z_{200} and $\mathsf{Z}_{200} - \mathsf{Z}_{1000}$ thickness onto the standardized $\mathsf{K}_{\mathsf{SST}}$ index, with negative (positive) lags denoting $\mathsf{Z}_{1000}/\mathsf{SST}$ and $\mathsf{Z}_{200}/\mathsf{Z}_{200-1000}$ anomalies leading (lagging) $\mathsf{K}_{\mathsf{SST}}$. The SST and $\mathsf{Z}_{200-1000}$ thickness fields are indicated in shading, and the Z_{1000} and Z_{200} fields are indicated by contours, where solid (dashed) lines indicate positive (negative) anomalies. Z_{1000} contours are spaced at 4 meters (-6, -2, 2, 6...m) and Z_{200} contours are spaced at 8 meters (-12, -4, 4, 12...m).

Figure 3: Statistical significance of the Z_{1000} (left column) and Z_{200} (right column) anomalies at a lag of (top) -30 days and (bottom) +30 days. Regressions are shown in contours and stippling indicates significance at the 95% confidence level using the two-tailed Student's t test. Degrees of freedom are calculated per Eq. (31) from Bretherton et al. [1999].

Figure 4: Daily lag regressions of SST (shading) and Z_{1000} (contours) onto the standardized $\mathsf{K}_{\mathsf{ATMO}}$ index. Z_{1000} contours with solid (dashed) lines represent positive (negative) values at an interval spacing of 10 meters (-15, -5, 5, 15...m). Positive lags indicate the fields lagging the $\mathsf{K}_{\mathsf{ATMO}}$ index.

Figure 5: Wintertime lag regressions of Z_{1000} and SST onto the standardized (left column) $\mathsf{K}_{\mathsf{SST}}$ index and (right column) $\mathsf{G}_{\mathsf{SST}}$ index. Negative (positive) lags denote the $\mathsf{Z}_{1000}/\mathsf{SST}$

406 anomalies leading (lagging) $\mathsf{K}_{\mathsf{SST}}$ and $\mathsf{G}_{\mathsf{SST}}$. The Z_{1000} field is indicated by contours (spaced
407 at 4 meters; -6, -2, 2, 6...m), where solid (dashed) lines indicate positive (negative) anomalies.

Figures

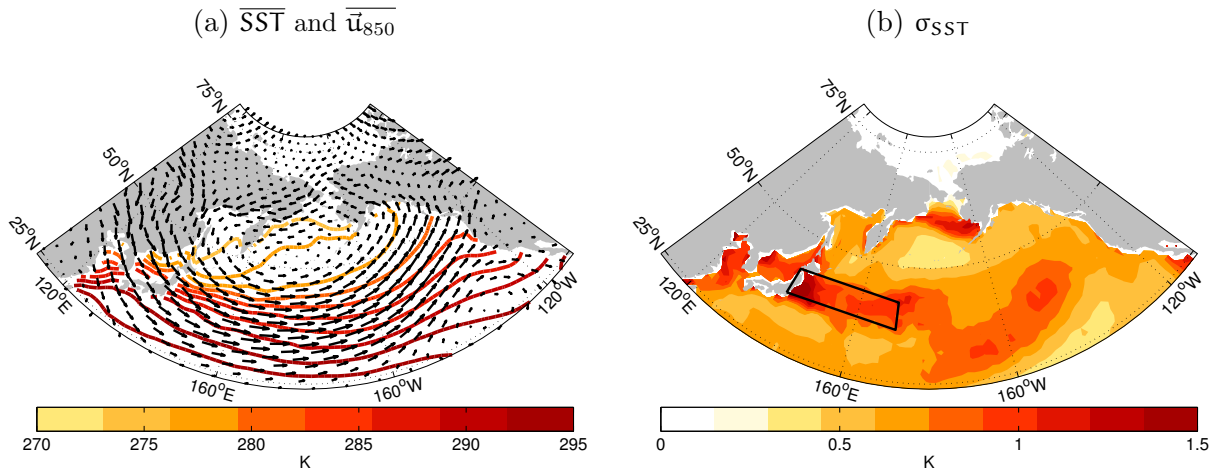

Figure 1: Climatological values of North Pacific wintertime (DJF) a) SST (contours) and $\vec{u}_{850}$ (vectors) and b) standard deviation of SST (σ_{SST}). The boxed region spans $36°N - 42°N, 140°E - 171E°$ and indicates the region used to calculate the K_{SST} index. Units for SST and σ_{SST} are in Kelvin. Units for $\vec{u}$ are in m/s.

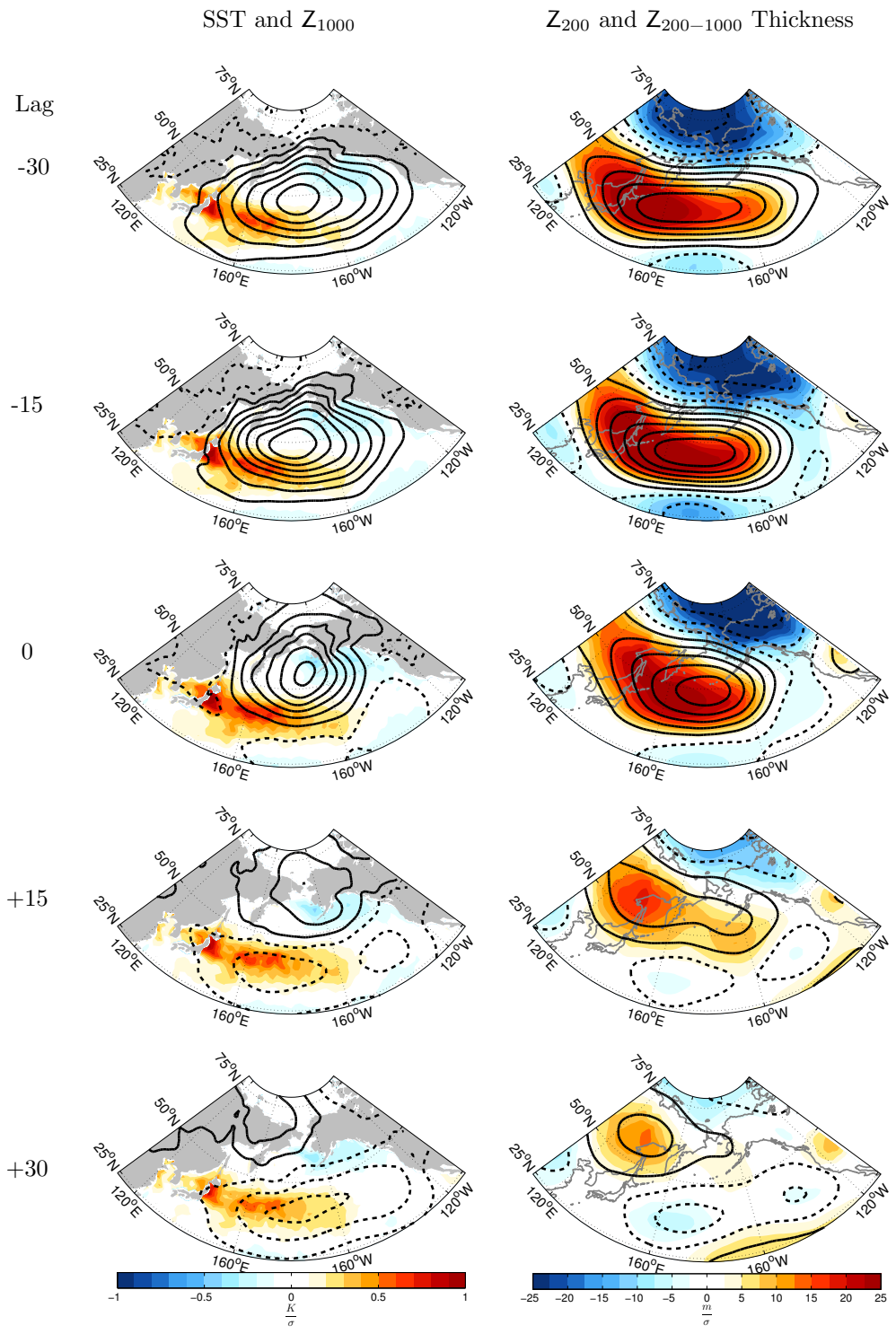

Figure 2: Wintertime lag regressions of (left column) Z_{1000} and SST and (right column) Z_{200} and $Z_{200} - Z_{1000}$ thickness onto the standardized K_{SST} index, with negative (positive) lags denoting Z_{1000}/SST and $Z_{200}/Z_{200-1000}$ anomalies leading (lagging) K_{SST}. The SST and $Z_{200-1000}$ thickness fields are indicated in shading, and the Z_{1000} and Z_{200} fields are indicated by contours, where solid (dashed) lines indicate positive (negative) anomalies. Z_{1000} contours are spaced at 4 meters (-6, -2, 2, 6...m) and Z_{200} contours are spaced at 8 meters (-12, -4, 4, 12...m).

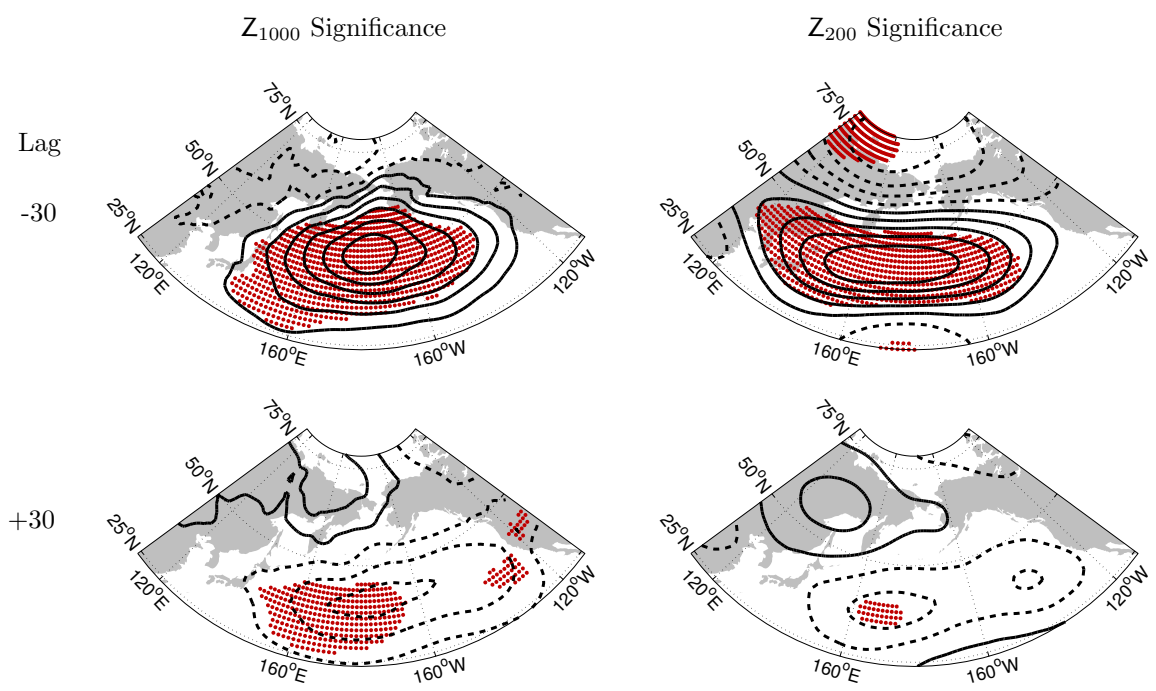

Figure 3: Statistical significance of the Z_{1000} (left column) and Z_{200} (right column) anomalies at a lag of (top) -30 days and (bottom) +30 days. Regressions are shown in contours and stippling indicates significance at the 95% confidence level using the two-tailed Student's t test. Degrees of freedom are calculated per Eq. (31) from Bretherton et al. [1999].

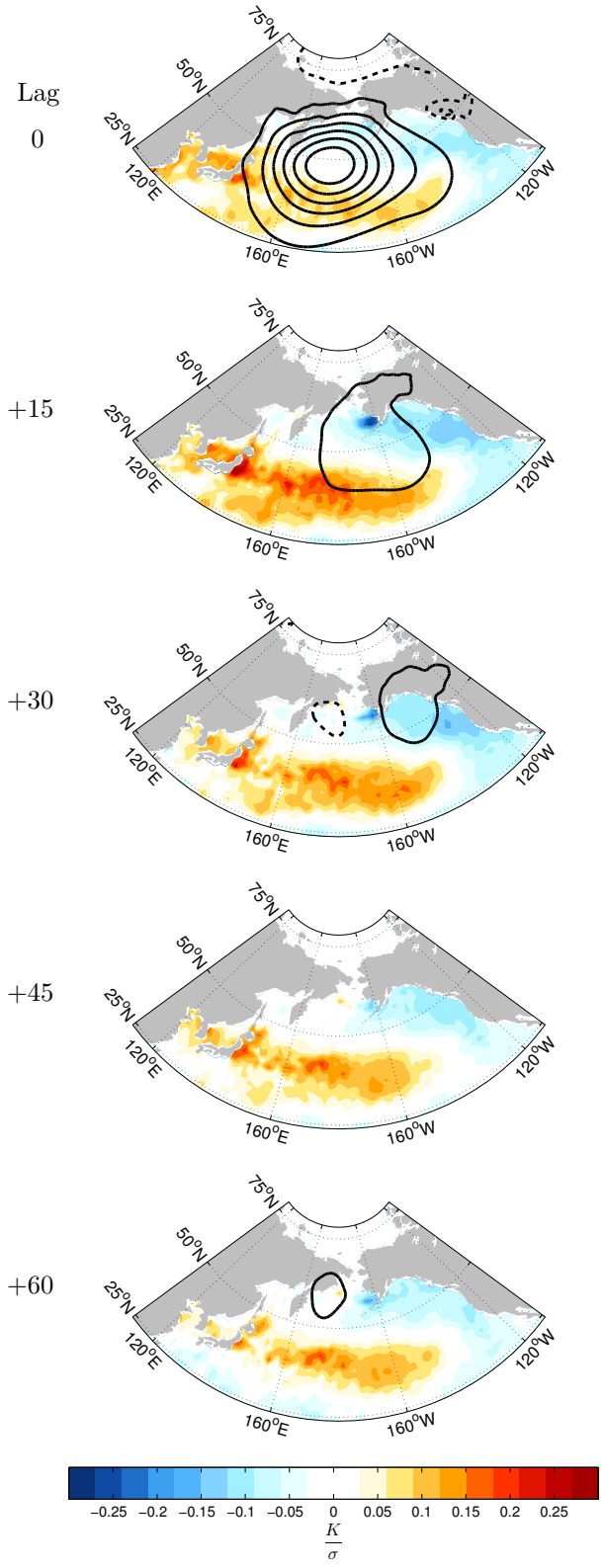

Figure 4: Daily lag regressions of SST (shading) and Z_{1000} (contours) onto the standardized K_{ATMO} index. Z_{1000} contours with solid (dashed) lines represent positive (negative) values at an interval spacing of 15 meters (-22.5, -7.5, 7.5, 22.5...m). Positive lags indicate the fields lagging the K_{ATMO} index.

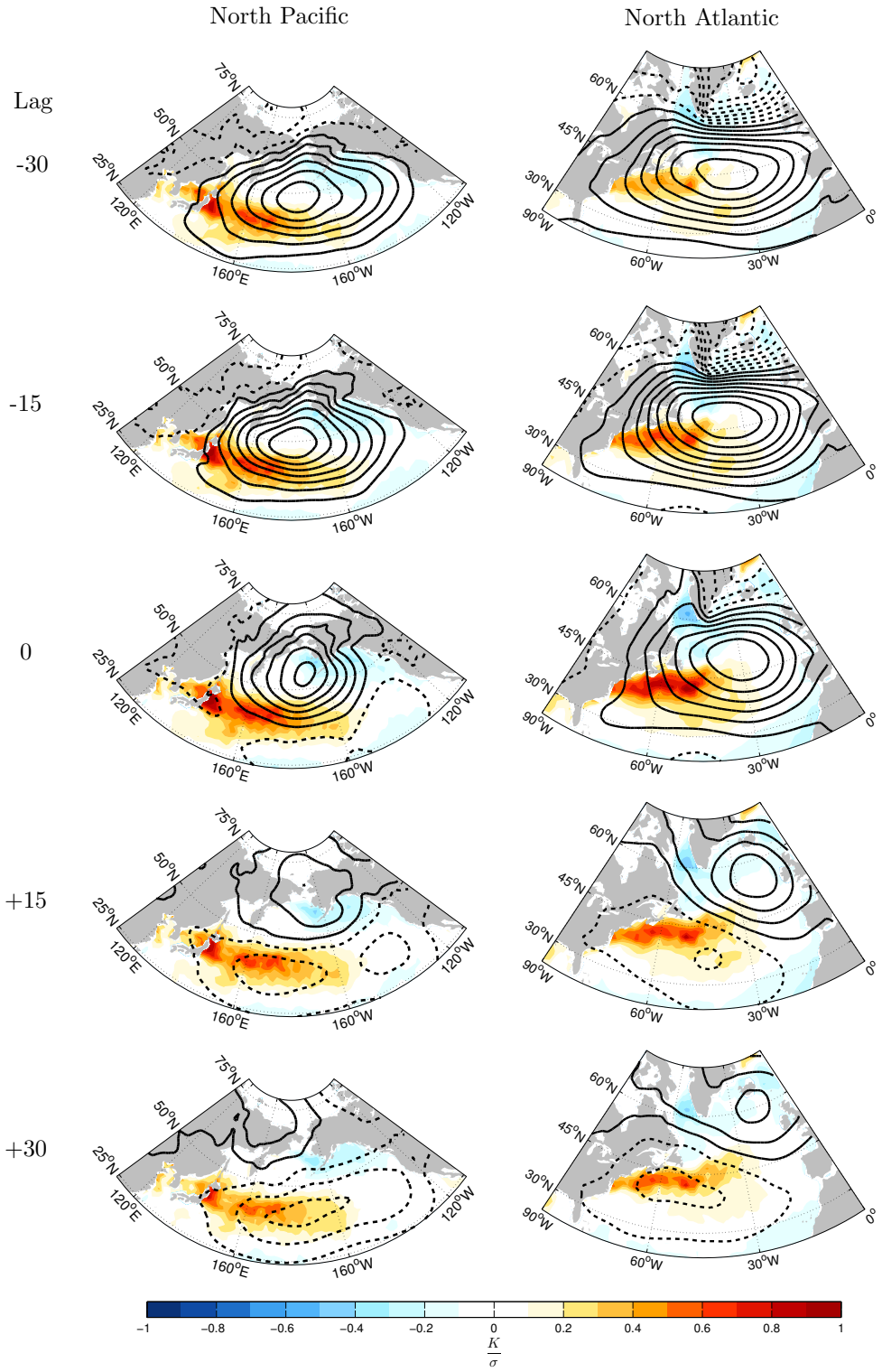

Figure 5: Wintertime lag regressions of Z_{1000} and SST onto the standardized (left column) K_{SST} index and (right column) G_{SST} index. Negative (positive) lags denote the Z_{1000}/SST anomalies leading (lagging) K_{SST} and G_{SST}. The Z_{1000} field is indicated by contours (spaced at 4 meters; -6, -2, 2, 6...m), where solid (dashed) lines indicate positive (negative) anomalies.